



Effective removal of industrial dye from aqueous solution using mesoporous nickel oxide: a complete batch system evaluation

Ghaferah H. Al-Hazmi^a, Moamen S. Refat^b, Mohamed G. El-Desouky^{c,*},
Farouk K.M. Wali^{d,e}, Ashraf A. El-Bindary^f

^aDepartment of Chemistry, College of Science, Princess Nourah bint Abdulrahman University, P.O. Box: 84428, Riyadh 11671, Saudi Arabia, email: ghalhazimi@pnu.edu.sa/dr.ghaferah@yahoo.com

^bDepartment of Chemistry, College of Science, Taif University, P.O. Box: 11099, Taif 21944, Saudi Arabia, email: msrefat@yahoo.com

^cEgyptian Propylene and Polypropylene Company, Port Said 42511, Egypt, email: ch.moh.gamal@gmail.com

^dChemical Technology Department, Prince Sultan Industrial College, Saudi Arabia

^eFaculty of Engineering, Mansoura University, Mansoura, Egypt, email: Farook19702001@yahoo.com

^fChemistry Department, Faculty of Science, Damietta University, Damietta 34517, Egypt, email: abindary@yahoo.com

Received 10 June 2022; Accepted 28 August 2022

ABSTRACT

Nickel oxide nanoparticles were synthesized via calcination of organometallic chelate. The adsorption of acid yellow 99 (AY99) was examined using produced NiO at temperatures of 450°C, 550°C, and 650°C. Different spectroscopic studies were used to characterize the synthesized NiO as an example (XRD) X-ray diffraction, FTIR, energy-dispersive X-ray spectroscopy (EDX), including the Brunauer–Emmett–Teller (BET) variable surface area, which was 156.036 m²/g. Scanning electron microscopy (SEM) got accustomed to quantifying the changes on the surface. Initial pH, for example, is variable to consider, the dose of adsorbent, time of contact, temperature, and the point of zero charging (pH_{pzc}) of NiO was designed and established to be 7.3. To discover the best adsorption conditions for extracting (AY99) from aqueous media, researchers looked into a variety of factors. Langmuir isotherm was shown to closely resemble the experimental values. To characterize the dye getting, the pseudo-second-order represents growth was adopted. This was also shown that adsorption has a high activation energy of 24.8 kJ/mol, this indicates that the adsorption obeys the chemisorption process. To determine adsorption equilibrium parameters, the Langmuir isotherm was utilized. Several thermodynamic constraints, for example, ΔG° , ΔH° , and ΔS° were calculated at various temperatures. The thermodynamics of the adsorption mechanism was discovered to be endothermic, random, and spontaneous. Compare the results of adsorption of AY99 over the NiO was 766.35 mg/g with other adsorbents and found it is the best one for removal.

Keywords: Adsorption; Isotherm; Kinetics; NiO nanoparticles; pH_{pzc}; Thermodynamics

1. Introduction

Manufactured plants like textiles, food, plastics, paper, tanneries, and cosmetics have all been colored using dyes [1]. The three types of dyes are cationic (basic dyes), anionic (acid dyes), and non-ionic (dispersed dyes). It is now crucial

from an environmental standpoint to treat wastewaters to eliminate colour. Because of their sulphonate groups, anionic dyes in aqueous solution have a net negative charge, whereas cationic dyes have a net positive charge because of their protonated amine or sulfur-containing groups. Therefore, it is essential to cleanse these discharge pigments

* Corresponding author.

before dispersing them in water. Additionally, because of their aromatic structure, they are more stable and more resistant to degradation.

The preponderance of dyes is organic compounds that are complicated that must be immune to a variety of factors, including detergent action. Synthetic dyes are commonly used in a variety of high-tech fields [2]. Textiles, papers, leather tanning, food manufacturing, polymers, cosmetic, latex, printing, and dye industries are just some of the industries involved. Groundwater tracing, determining activated sludge surface area [3], wastewater and pollution treatments, and other applications use synthetic dyes [4]. Because of their recalcitrance, releases from their outputs into the hydrosphere are a significant cause of pollution [5]. This will give the water a distasteful color, reducing sunlight penetration and making aquatic life more resistant to photochemical and biological attacks [6]. According to the most recent reports, over 100,000 industrial colors are available, with total yearly manufacturing of over 7,105 tons [7,8]. Over 10,000 tons of dye are consumed annually by the textile sector, and every year over 100 tons of dye are released into rivers [9]. A few of the processes being used to eliminate colours from wastewater Adsorption, coagulation, chemical oxidation, and membrane technology are some of the methods used [10]. Among the most effective modern wastewater management is adsorption, and it is used by companies to remove toxic inorganic and organic contaminants in effluent. In order to deal with dye pollution, many textile factories use industrial-activated carbon [11,12]. The current study focuses on the need for a low-cost, high-potential adsorbent to replace industrial activated carbon [13]. Many studies have focused on the feasibility of resources, manufacturing solid wastes, and agriculture by-products are all used and bio sorbents as forerunners for various low-cost adsorbents [14]. The lignin cellulosic biomass works well as an adsorbent [15]. The investigators also indicated that raw biomass adsorbents were subjected to various physical or chemical treatments to enhance their adsorption capacity [16–18].

Various methods, such as ozonation, have been successfully employed to remove different antibiotics from aqueous solutions [19–21], modern oxidation techniques, deterioration caused by photocatalysis [22,23], coagulation [24,25], and adsorption [26]. Nevertheless, it has many

challenges, such as poor performance, challenging operation, and harmful byproduct production [27,28]. Adsorption has the most promise among these techniques for the purification of water due to its ease of manufacture, low cost, great efficacy, and lack of harmful intermediates [29]. Water contaminants like activated carbon, metal oxides, clays, and agricultural wastes have all been removed using a variety of adsorbents. Furthermore, because natural adsorbents are inexpensive, researchers are concentrating depending on how frequently they are utilized in treating wastewater [30].

The goal of this work was the synthesis and characterized NiO nanoparticles in novel way that gives highly surface area 156.036 m²/g and effective removal of AY99 from wastewater 766.35 mg/g. And on other hand the reusability of NiO nanoparticles has its used about three times. The effectiveness of the removal of AY99 was compared with previous studies and the result referred that our adsorbent was the best than the other.

2. Material and methods

2.1. Materials and instruments

The materials and instrument used for characterization were illustrated in detail in (Supplementary material) [31].

2.2.1. Preparation of NiO nanoparticles

The NiO was obtained by calcination of [Ni(L)Cl(OH₂)₃] chelate at temperatures of 450°C, 550°C, and 650°C for 4 h. In addition, the dried NiO sample was sieved with a 200 µm mesh to obtain small uniform particles. This method produces NiO nanoparticles quickly and easily, without the use of expensive and harmful solvents or complicated equipment [32].

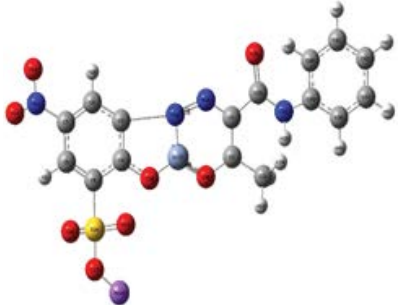
2.2. Preparation of adsorbate

AY99 with concentration (1 × 10⁻³ mol/L) was prepared using bidistilled water during the preparation of the stock solutions and the experimental study (Table 1).

2.3. Batch adsorption studies

Experimentation with pH (2–12) and other factors was studied by simply adding enough AY99 to distilled water

Table 1
Characteristics of adsorbate Acid Yellow 99 used in the study

Dye	Ball and stick model of dye	Molar mass (g/mol)	λ_{\max}	Electrical property
Acid Yellow 99		496.35	445	Anionic

to completely dissolve it, the effects of sorbent (NiO) dose concentration (0.01–0.1 g)/25 mL, The influence of NiO dosage on the adsorption of (AY99) in aqueous system and temperature (25°C–55°C) was examined [33]. Subsequent agitating at 200 rpm for 120 min, NiO was isolated by centrifugation. UV-Vis at 445 nm was used to assess the dye concentration. The proportion of decolorization (R) was determined from Eq. (1):

$$\%R = \frac{(C_0 - C_t)}{C_0} \times 100 \quad (1)$$

The adsorption potential (q_e , mmol/g) was calculated using the equilibrium equations (Eq. 2):

$$q_e = \frac{(C_0 - C_e)V}{M} \quad (2)$$

The total amount of dye per unit weight of the sorbent at time t was determined using the mass balance equation. (It explains why the amount of the solution has decreased) (q_t , mmol/g) as follows (Eq. 3):

$$q(t) = \sum_{i=1}^n \frac{[C(t)_{(i-1)} - C(t)_{(i)}] V(t)_{(i-1)}}{M} \quad (3)$$

3. Results and discussion

3.1. Characterization of NiO nanoparticles

3.1.1. X-ray diffraction (XRD) patterns

XRD was accustomed to investigating the purity and crystallinity of as-synthesized NiO nanoparticles, as shown in Fig. 1. The crystal planes (111), (200), (220), (311), and (222) of bulk NiO can be easily indexed at $2\theta = 37.20^\circ$, 43.20° , 62.87° , 75.20° , and 79.38° , respectively. Not just when it comes to peak position, but also when it comes to relative

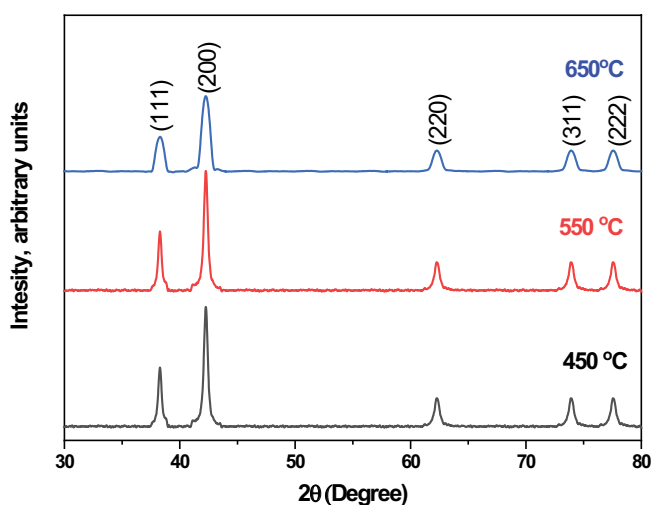


Fig. 1. NiO nanoparticles were analysed using XRD.

full strength. Each of these diffraction peaks is fully correlated with NiO's face-centered cubic (FCC) crystalline phase [33].

The calculated NiO lattice constant is 4.1729 \AA based on XRD measurements, which is in strong agreement with the data. (JCPDS, No. 04-0835). Applying Scherrer's formula $d = K/\lambda \cos\theta$, X-ray diffraction line broadening is used to assess the average crystallite size. Wherein d denotes grain size; $K = 0.89$ and λ is the wavelength of the X-ray (Cu Ka, 1.54056 \AA); NiO crystallinity size was determined Scherrer equation at (200) peak was 25, 42, and 60 nm at the temperatures 450, 550, and 650°C, respectively. It is obvious that when the temperature rises, the average particle size rises while the particular surface area decreases. The greater amount of NiO particle deposition can be used to explain these findings [34].

3.1.2. Brunauer–Emmett–Teller (BET) surface area

Because the size and number of pores can significantly affect a substance's properties and its capacity for process, in a porous material, determining the effective surface area of the holes is extremely important. This is commonly accomplished by measuring the material's Brunauer–Emmett–Teller (BET) area of contact. Surface interactions occur whenever a gas interacts with a substance's outer surface. Physisorption-based adsorption isotherms and the likelihood that gas will get weakly attached to a substance's surface serve as the foundation for BET tests. Gas can quickly adsorb and desorb from the surfaces of a substance since physisorption is reversible.

The adsorption isotherm, which measures volume, is produced when gas is adsorbed while being subjected to a range of pressures and temperatures. The temperature is roughly 77 K since liquid nitrogen is employed to maintain the temperature's stability. Plotting the quantity of gas adsorbed against the results of the relative pressure in the complete graph of the adsorption isotherm. The concave shape of the plot shows the type of porosity existing in the substance (Fig. 2) as well as the sort of pores in the

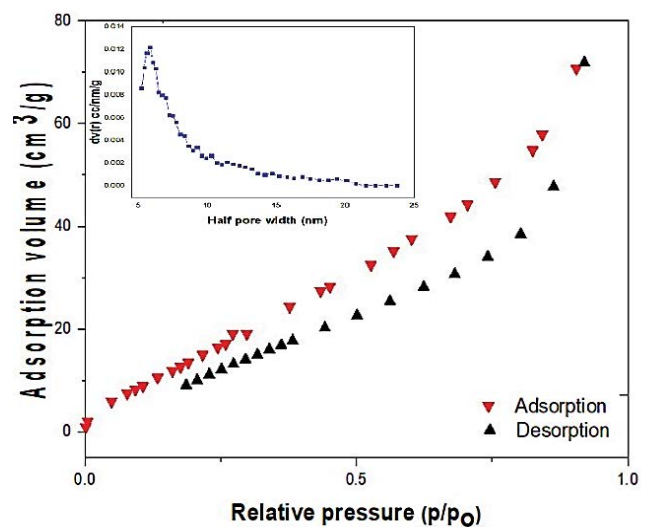


Fig. 2. NiO at 450°C isotherms of N_2 adsorption/desorption.

substance (Table 2). The presence of a hysteresis loop is shown by type IV adsorption isotherms for NiO restricted absorption at high initial P/P₀ and capillary condensation in a mesoporous medium. The first loop is responsible for mono-multilayer adsorption, while the second is responsible for desorption. Adsorption effectiveness of the sample calcined at 450°C is higher in our case. Which has a lower crystallite size and a larger specific surface area than the others (156.036 m²/g) [12].

3.1.3. SEM analysis

The surface properties of NiO nanoparticles were examined using SEM (Fig. 3) depicts the uniform development of metal oxide. The cultivated nanostructures are in the form of nanoparticles that were interlinked and created pores

Table 2
NiO nanostructures' average pore size, surface area, and volume of pores

Average pore size (nm)	Pore volume (cm ³ /g)	Specific surface area (m ² /g)	Temperature (°C)
3.485	0.1890	156.036	450
5.058	0.4582	87.121	550
9.681	0.7054	33.800	650

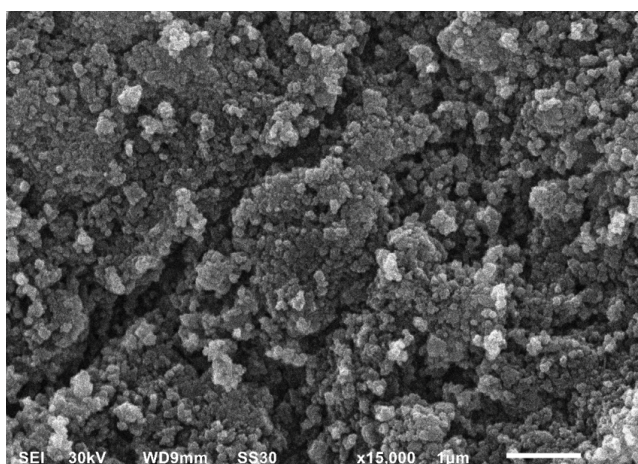


Fig. 3. NiO at 450°C is shown in an SEM picture.

and fissures, resulting in vast surface areas for rapid dye dispersion on metal oxide surfaces, SEM photos at greater microscopy demonstrate this. NiO nanoparticles having a diameter ranging from 27 to 47 nm were approved by SEM examination [35,36].

3.1.4. Energy-dispersive X-ray spectroscopy (EDX)

Owing to its atoms, each material will have its X-ray spectrum with its unique set of peaks, according to energy dispersive X-ray analysis. To evaluate the chemical contents of nanoparticles, EDX studies were employed. Peaks for Ni and O were discovered, but no peaks for impurities, suggesting that NiO had been clean for a long period (Fig. 4) [35].

3.2. Batch experiments

3.2.1. Determining the point of zero charge (pH_{PZC})

pH_{PZC} was one of the most important variables in the destruction of AY99. The charge on the surface of NiO was measured, as well as ionic species contained in the adsorbate solution (Fig. S2). The pH (pH_{PZC}) where the positive and negative charges at surfaces are equivalent is known as the PZC. The surface charge of NiO was determined using this method. The pH_{PZC} of NiO was found to be 7.3. This demonstrates that NiO obtains a positive charge under this one pH as a result of functional group protonation, because of protonation of functional groups, NiO gets a negative charge above this pH [37,38].

3.2.2. Effect of pH

Absorption of AY99 as a function of pH in the starting solution onto NiO may be seen in Fig. 5 (1.2 × 10⁻³ mol/L, 25°C and dosage 0.02 g/25 mL, contact time 60 min). For dye adsorption, a low pH appears to be most efficient. The dye's absorption was found to be inhibited at higher pH levels. Because the adsorbent has a structural alteration that corresponds to the dye charge, electrostatic repulsions are assumed to be what causes the dye absorption to drop [39]. When the pH is lower, to combat the dye, there are usually more protons (H⁺) in the solution. The positive charge of the NiO surface was demonstrated to decrease as the pH of the solution raised, which harms dye absorption Fig. S2. As a result of this dye's removal, NiO nanoparticles are an efficient adsorbent, with a pH of 4

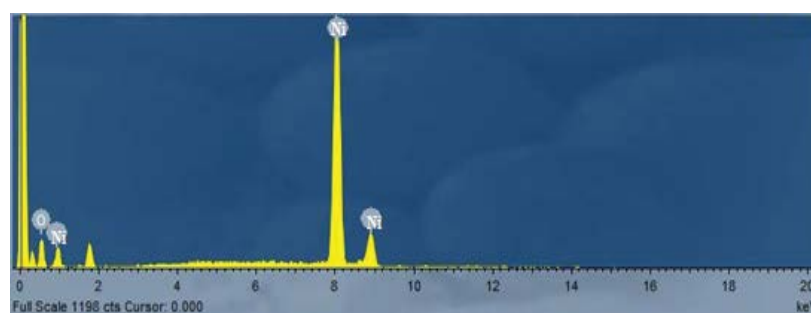


Fig. 4. NiO's EDX spectrum at 450°C.

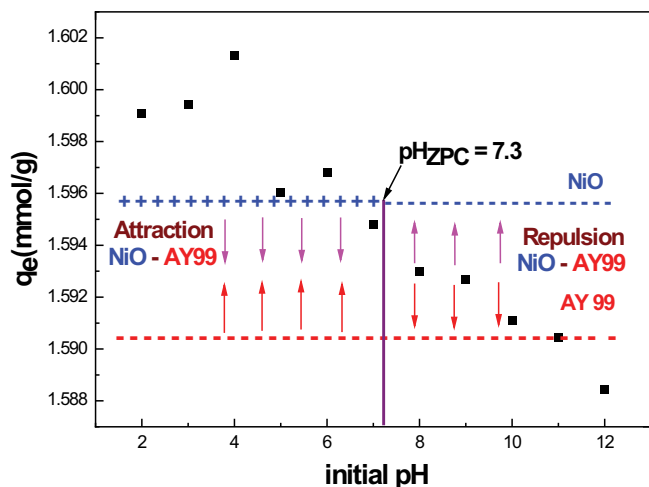


Fig. 5. pH's impact on AY99's adsorption on NiO.

being the best. A negatively charged adsorbent surface is produced as the pH rises due to a decrease in the positive charge on the oxide or solution contact. Higher OH ion concentrations and ionic repulsion between anionic dye molecules and the negatively charged surface could be the cause of lower adsorption at high pH values. Adsorption is decreased at higher pH values because the outer layer of the adsorbent doesn't contain any substitutable anions. Adsorption of anionic dyes is best at $\text{pH} < \text{pH}_{\text{pzc}}$ where the NiO has a positive charge [40,41].

3.2.3. Effects of calcination

Researchers looked examined the impact of NiO calcination temperatures of 450°C, 550°C, and 650°C on AY99 adsorption studies. NiO dose was 0.02 g; the volume of dye solution was 25 mL; and concentration was 1.2×10^{-3} mol/L, the pH level was 4, and the shake velocity was 200 revolutions per minute. The effectiveness of NiO adsorption increased when the calcination temp was lowered $1.239 > 1.38 > 1.4516$ mmol/g for NiO at calcination temperature 450°C, 550°C and 650°C, respectively (Fig. 6) [42,43].

3.2.4. Influence of NiO dosage

By varying the adsorbent ranges, the AY99 adsorption of NiO nanoparticles substance was investigated (0.01–0.1 g) per 25 mL, AY99 concentration of 1.51×10^{-3} mol/L at 25°C and pH 4. The graph below displays the adsorption capacity of AY99 as a percentage of the amount of adsorbent (Fig. 7a). The capacity of AY99 adsorption reduces as the dosage of NiO is raised from 1.06 to 0.28 mmol/g and rises from 0.01 to 0.1 g per 25 mL. The nickel oxide dose effect on optimum concentration (C/C_0) of AY99 is seen in Fig. 7b. As the dosage increases, with increasing adsorbent surface area, the equilibrium concentration of (AY99) declines [44].

3.2.5. Influence on initial dye concentration (C_0)

On NiO nanoparticles, the effect of the concentration of AY99 initially was looked into using an AY99 concentration

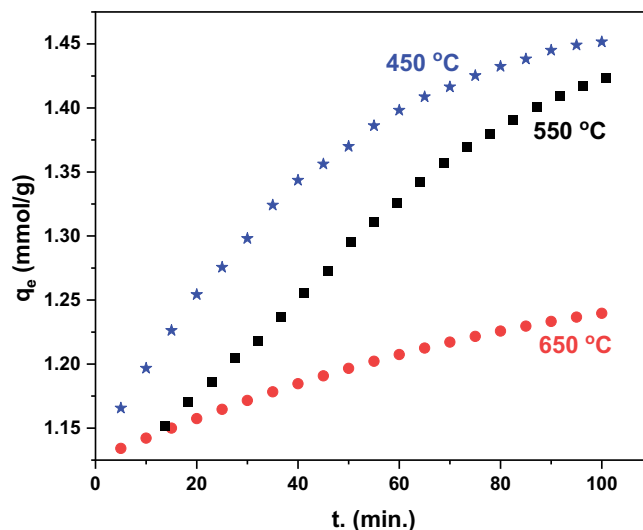


Fig. 6. NiO calcination temperature's impact on AY99 adsorption (T : 25°C; pH : 4; C_0 : 1.2×10^{-3} mol/L).

of 6.7×10^{-4} to 1.4×10^{-3} mol/L and a NiO dose of 0.02 g. The removal percentage was reduced as the initial AY99 concentration was raised. At greater AY99 concentrations, the active functional groups of NiO as a result of saturation, adsorption decreases. At higher AY99 concentrations, the removal efficiency was lower (decreasing from 99.8% to 88.7% with an increase in AY99) [45]. The most common cause is an increase in the surface charge on NiO. As a result of this saturation, the active sites became saturated, lowering the dye removal quality. The higher AY99 starting concentration might be explained by the improved NiO that was present with the enhanced adsorbent-dye interaction (Fig. 8) [46,47].

3.2.6. Adsorption isotherms

AY99 absorption on NiO was computed utilizing isotherm models such as Langmuir [48], Freundlich [49], Temkin [50], Dubinin, and Radushkevich [51]. The best fit was picked based on the R^2 about one. The results of the isotherm modeling are summarized in (Table 3). Langmuir isotherm model the best fit (Fig. 9). This indicates the presence of a monolayer adsorption process 1.527 mmol/g was the monolayer adsorption potential (q_m) and 24.8 kJ/mol is the average sorption energy value. In respect to the chemisorption process that has been suggested, this is accurate. Indeed, the limit energy for separation is generally agreed to be 8 kJ/mol. Chemical sorption (up to 8 kJ/mol) and physical sorption (below 8 kJ/mol).

3.2.7. Adsorption kinetics and mechanism studies

Uptake AY99 onto NiO was modeled using the pseudo-first-order (PFO) [53], pseudo-second-order (PSO) [54], intraparticle diffusion, and Elovich kinetic models in this study. The coefficient of determination (R^2) value was used to find the best fit. The PFO and PSO models were unable to specify governing diffusion mechanisms, hence

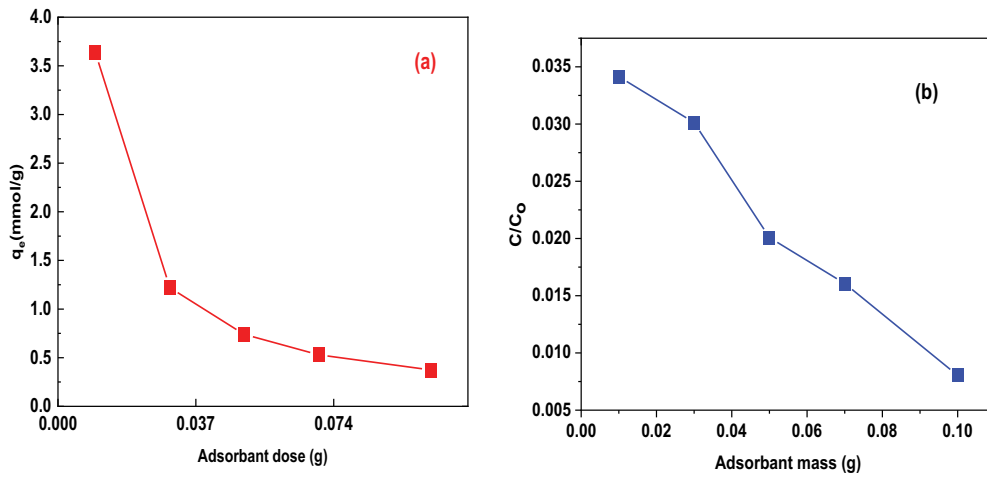


Fig. 7. The effects of NiO dosage on the adsorption of AY99 at (T : 25°C; pH: 4; C_0 : 1.51×10^{-3} mol/L) are as follows: (a) Capacity of absorption vs. NiO dosage and (b) NiO dosage vs relative residual concentration (C/C_0).

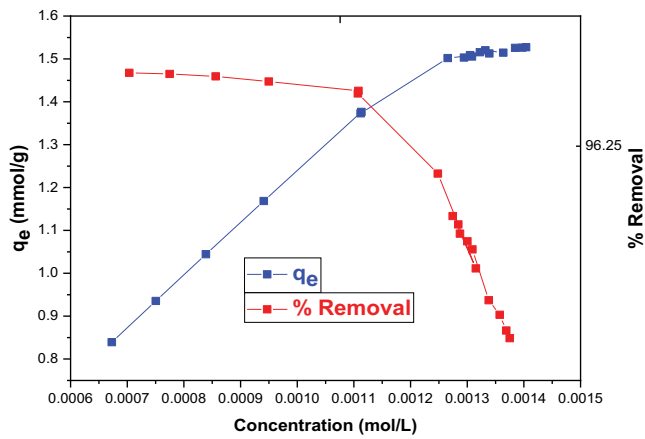


Fig. 8. According to the initial dye concentrations, AY99 adsorption onto NiO was studied (T : 25°C; pH: 4; C_0 : 6.7×10^{-4} to 1.4×10^{-3} mol/L).

an intraparticle mass transfer diffusion model was utilized instead [55].

Table 4 summarizes the findings of the kinetics modeling and displays the intraparticle diffusion equilibrium constant (K), PFO constants (K_1), and PSO constants (K_2). Due to its properties, For the adsorption mechanism, the PSO is the ideal fit R^2 equals 0.999 is comparatively a greater correlation coefficient (R^2). Designates in the kinetics of absorption, the accessibility of binding sites as well as the quantity of dye in liquid are important considerations. The intraparticle diffusion kinetic modeling ($R^2 = 0.1999$) for AY99 was calculated using the slope of the second-linear region that corresponds (Fig. 10). The external barrier to mass transfer around the particles is most important during the early stages of adsorption (initial sharp rise). The second equation portion intraparticle diffusion technique for continuous adsorption. If the plots not intersect at the beginning, this demonstrates that porosity dispersion is not only a rate-limiting stage; Extra simulations can control the adsorption rate as well,

Table 3
Adsorption of AY99 onto NiO isotherms parameters and their correlation coefficients [8,52]

Isotherm	Value of parameters	
Langmuir	$q_{m,exp}$ (mmol/g)	1.527
	q_m (mmol/g)	1.536
	K_L (L/mmol)	6.2E+05
	R^2	0.99952
Freundlich	n	9.362
	K_F (mmol/g) (L/mmol) ^{1/n}	4.013
	R^2	0.877
Dubinin–Radushkevich	q_{DR}	0.834
	K_{DR} (J ² /mol ²)	-8.14E-10
	E_a (kJ/mol)	24.8
	R^2	0.9068
Temkin	b_T (L/mol)	19,081.73
	A_T (kJ/mol)	20.72
	R^2	0.91

which are both capable of working in tandem [56,57]. As the adsorption sites of NiO are heterogeneous, the Elovich equation suggests a wide variety of activation energies for chemisorption. Parameter α (associated to the proportion of chemisorption) as the amount of dye in the solution increases, the parameter (which was proportional to the coverage surface) is reduced (Table 4), this is because the useful adsorption surface of the adsorbate has decreased [57]. As a result, by raising the concentration within the range under study, chemisorption can occur more quickly. The excellent accuracy of the pseudo-second-order kinetic model makes it useful for simulating adsorption kinetics. Its foundation is the idea that the frequency stage involves electrostatic chemisorption as a result of the adsorbent and adsorbate sharing or exchanging electrons [58,59].

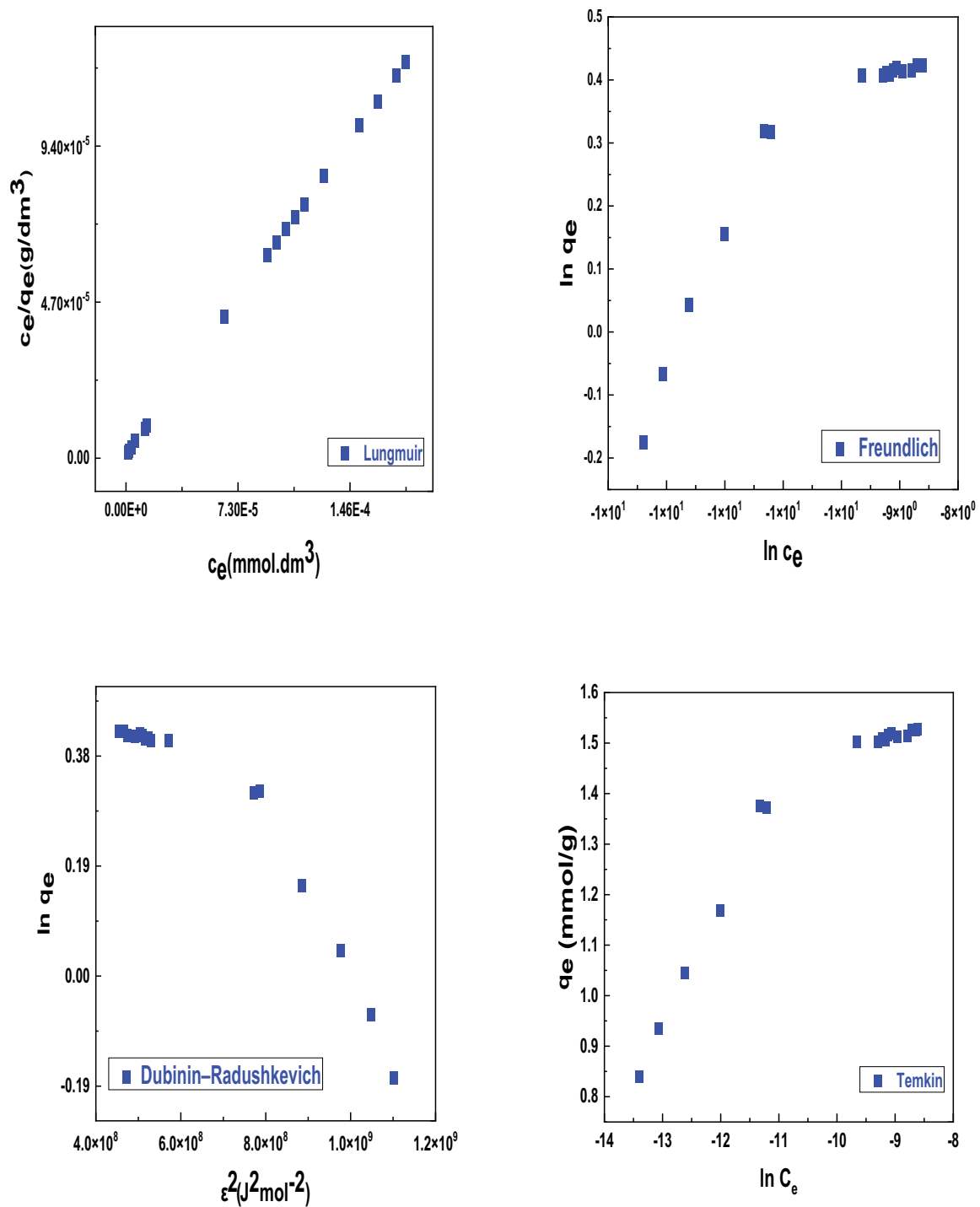


Fig. 9. Plots for AY99's linearized isothermal sorption (T : 25°C; pH: 4; time: 45 min; C_0 : 1.51×10^{-3} mol/L).

3.2.8. Experimental isotherms are adjusted using theoretical models

To find the best statistical physics model that correlates well with empirical adsorption isotherms. To verify the empirical isotherms, we use mathematical software. The Levenberg Marquardt algorithm of iteration that used multivariate non-linear regression Software is a widely used

mathematical tool for altering the results of the experiment using a predetermined model [42]. The best-fitting models are evaluated using three error factors. The first is the R^2 evaluation coefficient, which indicates how well the fit is; The RMSE (residual root mean square error) is the second criterion, and the third is the Akaike information criterion (AIC). The following are examples of situations that imply that a proposed model matches the results of the experiment

Table 4
The kinetics of AY99 adsorption onto NiO nanoparticles and the correlation coefficients for that process [8,52]

Model	Value of parameters	
Pseudo-first-order kinetic	K_1 (min ⁻¹)	0.016
	q_e (mmol/g)	0.28
	R^2	0.822
Pseudo-second-order kinetic	K_2 (g/mg·min)	7.49
	q_e (mmol/g)	1.49
	R^2	0.9999
Intraparticle diffusion	K_i (mg/g·min ^{1/2})	-0.069
	X (mg/g)	0.552
	R^2	0.1999
Elovich	β (g/mg)	-4.065
	α (mg/g·min)	2.715
	R^2	0.3587
Experimental data	q_e (exp) (mmol/g)	1.4898

effectively: Because R^2 approaches toward agreement, restriction values are inside ± 2 RMSE of their true results. Furthermore, The AIC coefficient should be kept to a bare minimum. Table 5 shows the R^2 , RMSE, and AIC coefficients obtained utilizing adsorption methods to change the observed isotherms. We conclude depending on the coefficient value obtained by each model following the conclusion.

The Adsorption Kinetic and isotherm models were selected as suitable models for the adsorption of AY99 on NiO as error factors obeyed the standards (The R^2 value is the highest, while the RMSE and AIC values are the lowest). Therefore, it is suggested that the AY99 adsorption on NiO is regulated by the negatively charged dye ion's electrostatic interaction with the positively charged NiO surface. Anionic dye is represented by AY99. The dye decomposes into two components in an aqueous solution to (SO_3^-) and (Na^+) (Table 6).

3.2.9. Thermodynamic modelling studies

The change in free energy (ΔG°), enthalpy (ΔH°), and entropy (ΔS°) were computed using thermodynamics modeling to investigate several characteristics of NiO's adsorptive elimination of AY99. In Table 6, the results of thermodynamic modeling at various temperatures are enumerated. As (ΔG°) is negative, the process is both possible and randomized. (ΔG°) values fell from -8.27 to -11.23 kJ/mol at elevated temperatures. As a result, the removal of AY99 from NiO becomes more appealing. ΔG° may be seen to be linear when plotted against temperature T (Fig. 11) (ΔH°), and (ΔS°) 26.35 and 0.118 kJ/mol, respectively, were determined. The presence of positive ΔH° values indicates that the adsorption mechanism is endothermic. A positive value of (ΔS°) identifies the existence of structural reforms on the NiO throughout the absorption of AY99. The quantity of randomization at the solid-liquid contact grows. Additionally, the positive number suggests that the NiO adsorbent has a strong affinity for AY99 [52].

The adsorption cycle's slope and intercept were calculated using the $\ln K_c$ vs. $1/T$ plot's standard (ΔH°) and

(ΔS°) was determined. Arrhenius plot intercept was used to compute E_a (Fig. 12). The amount of ΔH° in adsorption processes is positive, indicating an endothermic reaction. While (ΔG°) negatively, it designates spontaneous reaction (Table 6) [57]. In this scenario, the zero standard free energy temperature (T_0) is calculated to be 223 K for AY99. The adsorbents examined are functional and can absorb colorants at very low temperatures, as seen by the low T_0 values [60].

According to the Van't Hoff plot (Fig. 12), the values of ΔG° , ΔS° , and ΔH° for the AY99 adsorption on NiO are calculated with coefficients of detection equal to 0.997. The fact that there were always negative ΔG° quantities (Table 6) as the temperature rose from 298 to 318 K showed that the adsorption approach is spontaneous and more effective at higher temperatures. The adsorption mechanism is said to be spontaneous based on the negative numbers of ΔG° . The mechanism becomes more advantageous at higher temperatures in the examined temperature range, as seen by the rise in the negative values of ΔG° with rising temperature. The AY99 dye molecule interacts with the NiO adsorbent in an endothermic manner, as shown by the positive value of ΔH° for AY99 adsorption (26.35 kJ/mol). A growth in disorder or randomization at the solid-liquid interface is suggested by the affirmative statement that even during the adsorption process. The data in Table 6 similarly show that the values of $T\Delta S^\circ$ rose as the temperature rose and $|\Delta H^\circ| < |T\Delta S^\circ|$. This demonstrates that the adsorption reaction exhibits more entropy change than enthalpy change.

3.2.10. Effect of ionic strength (addition of NaCl)

In addition to NaCl (C_0 : 1.51×10^{-3} mol/L; NiO dosage: 0.02 g/25 mL), The influence of Cl^- on the extraction of AY99 was studied. As the amount of NaCl in the solution is increased, the effectiveness of adsorption is slightly reduced. When the quantity of sodium chloride in the water is 20 g/L, a 20% reduction in absorption capability is required [61]. This might be a result of competition between the AY99 anions and the chloride anions for the sorption sites. The adsorption process declines by 1.5% even at a NaCl concentration of 40 g/L, indicating possibility is maintained in the face of difficulty (Fig. 13) [52].

3.2.11. Mechanism of interaction

The maximum AY99 adsorption was discovered to take place at pH_{pzc} of NiO adsorbent values that are less than 7.3. AY99 absorption, As an approach, a pseudo-second-order kinetic model based on intraparticle diffusion is used. It might be explained by the effects of the initial pH of the sorption solution on the surface chemistry of NiO and the properties of the ionized adsorbate molecules. The main active principle might be the energy of the interaction between the charged AY99 molecule and the NiO surface. Through experimental analysis, the pH_{pzc} of the NiO adsorbent was determined to be 7.3. The number of positive charge places increases while the number of negative charge positions decreases as the pH of the system decreases. Electrostatic interaction improves adsorption on the NiO nanoarchitecture's negative charge surface. At

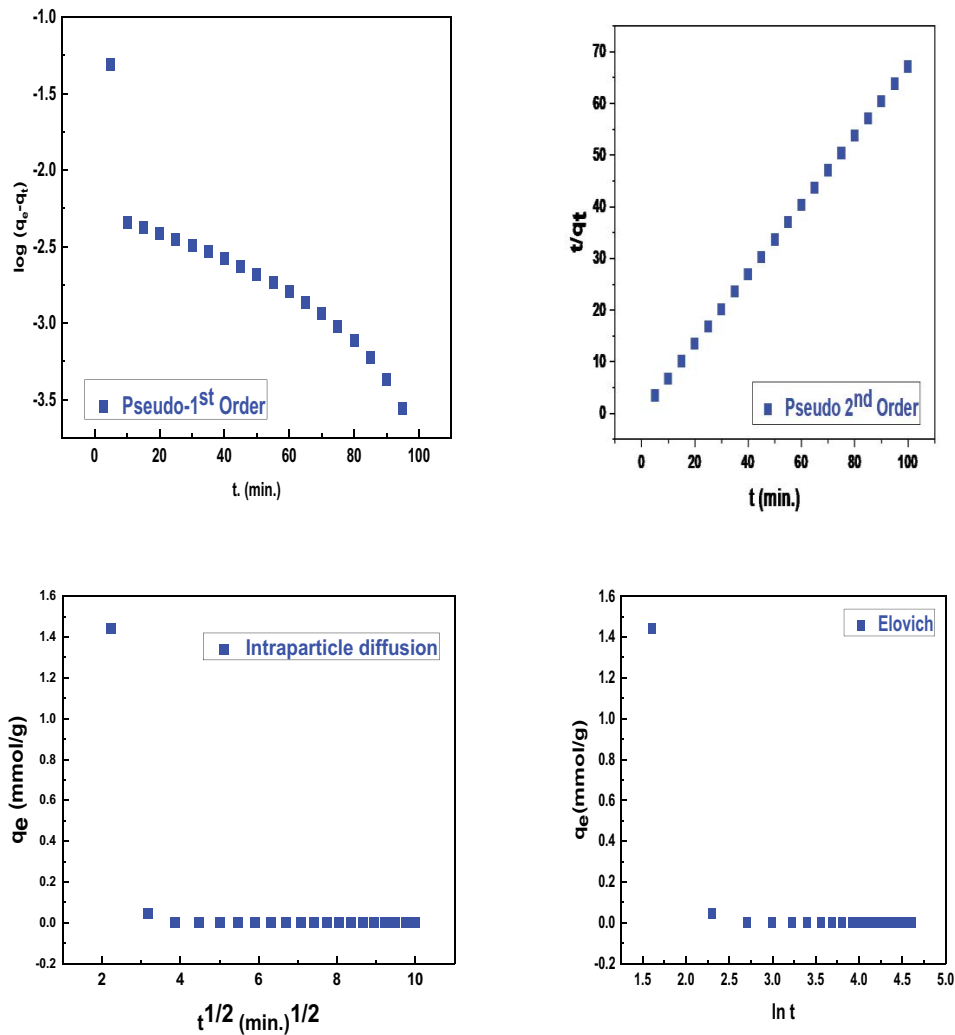
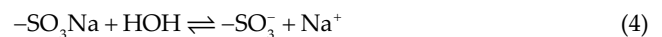


Fig. 10. Modeling of AY99's uptake kinetics (T : 25°C; time: 100 min; pH: 4; C_0 : 1.51×10^{-3} mol/L).

Table 5
Comparison between R^2 , RMSE and AIC coefficient

Adsorption models	R^2	RMSE	AIC
Langmuir	0.999	0.822	10.04
Freundlich	0.877	1.89	8.42
Dubinin–Radushkevich	0.906	1.05	9.59
Temkin	0.91	3.56	7.15
Pseudo-first-order	0.822	2.4	7.9
Pseudo-second-order	0.9999	0.923	9.85
Weber	0.199	0.6	10.68
Elovich	0.358	0.95	9.7

acidic pH, excess Ni^+ ions also exist and the chosen anionic dye is more readily adsorbed. The ($-\text{SO}_3^-$) on AY 99 and the positive sites on the adsorbent are attracted to each other by electrostatic forces. Ni^+ and dye molecules' positive cations may exchange ions, and dye adsorption onto NiO may also result from pore filling in [8].



3.2.11.1. Active sites

The method of analyzing the adsorption groups the electrophilic/nucleophilic attacking region and the electrostatic potential zero zones in the investigated AY99/NiO systems is referred to as molecular electrostatic potential (MEP). In this study, utilizing molecular electrostatic potentials, the entire electron density surface of AY99 was charted (MEP) (Fig. 14). Different shades were used to indicate the MEP's various values in these maps (red, yellow, green, light blue, and blue). Indeed, Negative MEP results were shown by red and yellow colours, which are connected with electrophilic; positive MEP levels were shown by blue colours,

Table 6
 ΔG° , ΔH° , and ΔS° for the adsorption of AY99 on NiO

Dye	T (K)	ΔH° (kJ/mol)	ΔS° (J/mol·K)	E_a (kJ/mol)	T° (K)	$-\Delta G^\circ$ (kJ/mol)
AY99	298	26.35	118	1.15	223	8.27
	303					8.69
	308					9.46
	313					10.05
	318					11.23

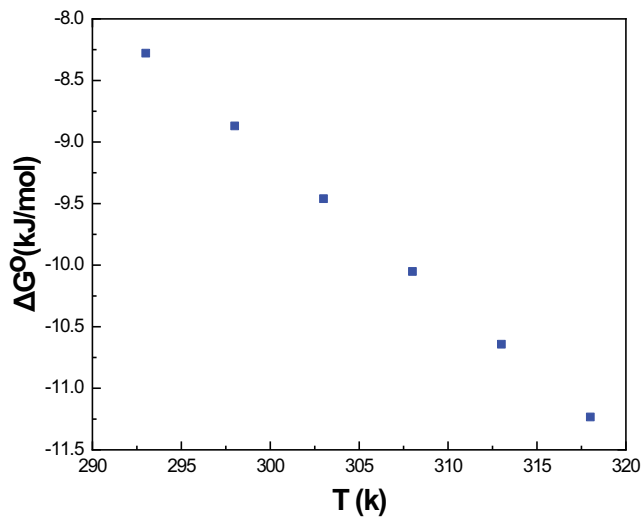


Fig. 11. The graph displays how Gibbs free energy (ΔG°) varies with temperature (T : 25°C; pH: 4; time: 30 min; C_0 : 1.51×10^{-3} mol/L).

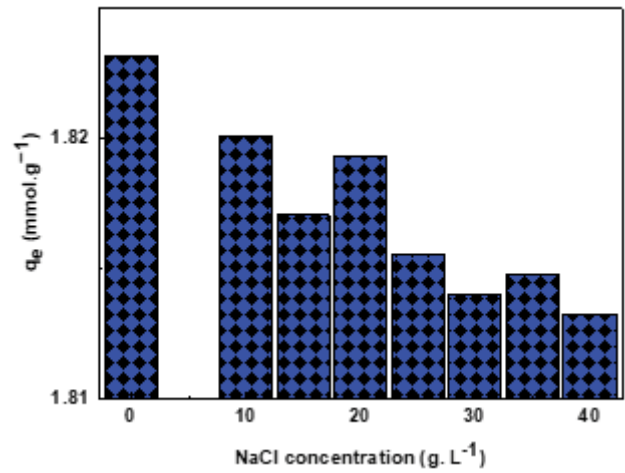


Fig. 13. NaCl's impact and the adsorption of AY99 on NiO nanoparticles (T : 25°C; pH: 4; time: 30 min; dose: 0.02 g; C_0 : 1.51×10^{-3} mol/L).

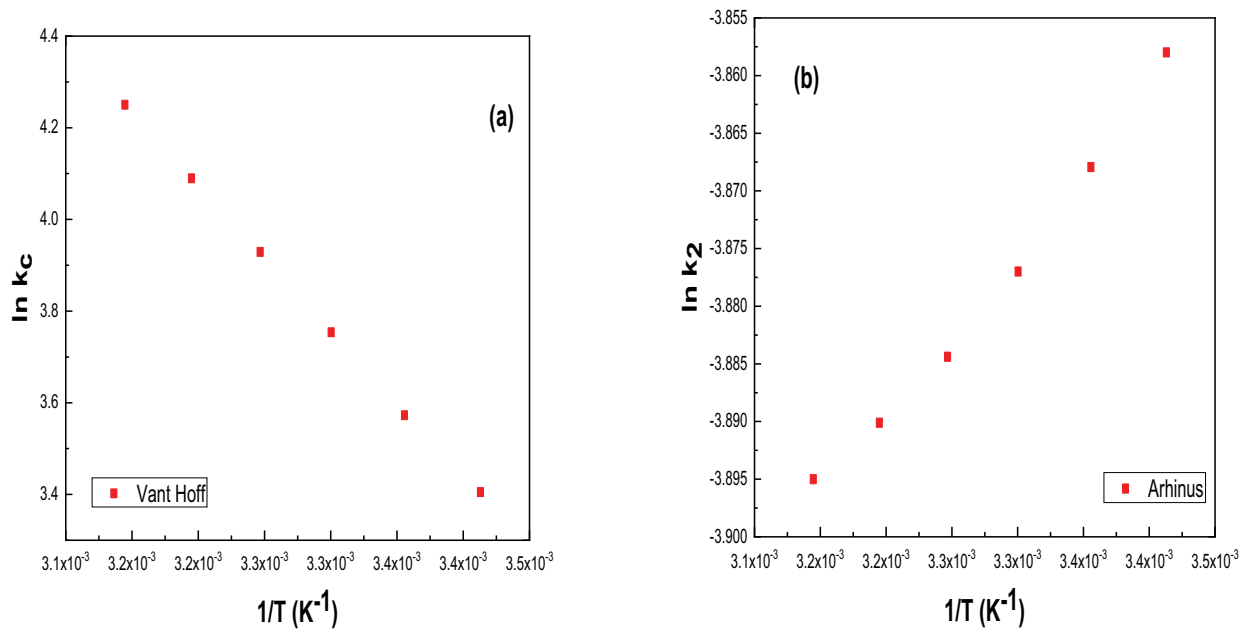


Fig. 12. (a) The NiO adsorbent is the subject of a Van't Hoff plot for AY99 adsorption. (b) AY99 adsorption onto the NiO adsorbent is shown on an Arrhenius plot. At (T : 25°C; pH: 4; time: 30 min; C_0 : 1.51×10^{-3} mol/L).

which are linked with nucleophilic attack; and the MEP zero area is symbolized by green. As seen in the AY99 map, the MEP of AY99 indicates that is most susceptible to nucleophilic attack (Fig. 14). In addition, the MEP map exposes that the AY99 approves that the adsorbate is typically favorable to nucleophilic attack [62].

On the other hand, have known active binding sites. As a result, if these groups are present, they will boost dye adsorption, yet the adsorption findings revealed the following: NiO adsorbent capacity in regards to AY99 adsorption capacities is owing to that contact in between Delocalized–electrons in NiO planes and free electrons in AY99 molecules positioned in aromatic rings or numerous bonds [63].

Table 7 shows the E_{HOMO} and E_{LUMO} principles, and the energy disparity between all compounds, $E_{\text{LUMO-HOMO}}$. The difference in energy can be used to find out how hard molecules are and how soft they are (Fig. 15) [64]. Because the molecule has a reduced volume of energy. It is more polarizable and less powerful (more reactive). AY99 Quantum chemical descriptions were identified as chemical potential (μ), electronegativity (χ), global softness (σ), global hardness (η) and electronegativity (χ), global hardness (σ), Global index of electrophilicity (ω).

Indeed, theoretically, the E_{gap} is defined as a major reactivity of chemicals component of AY99, a tiny gap denotes a high level of chemical reactivity (poor stable), a huge gap, on the other hand, suggests low chemical reactivity (highly stable) (Table 7).

3.2.12. Comparison with other adsorbents

Table 8 compared the maximal AY99 adsorption capacities of NiO to those previously reported for those other adsorbent materials. It demonstrates that the NiO produced has a significant capacity for AY 99 adsorptions.

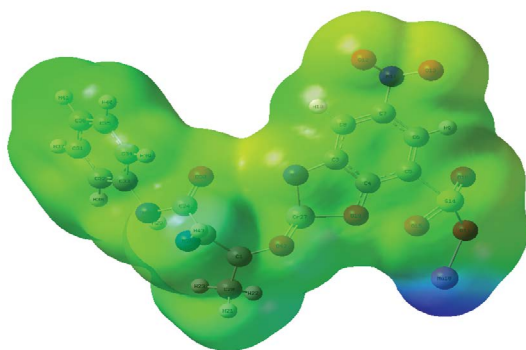


Fig. 14. AY99's molecular electrostatic potential (MEP).

Table 7

Quantum chemical characteristics of the AY99 under examination were established

Comp.	E_{HOMO} eV	E_{LUMO} eV	ΔE eV	X eV	η eV	Pi eV	σ eV ⁻¹	S eV ⁻¹	Ω eV	ΔN_{max}
AY99	-0.203	-0.143	0.068	0.173	0.03	-0.17	33.33	16.66	0.49	5.7

3.2.14. Desorption studies

Adsorbent's capacity to regenerate with its constancy is two important issues that influence its practical application. We've now compared NiO's adsorption potential over three adsorption–desorption cycles in a row [43]. The examined sorbent NiO was washed several times with ethanol until colorless, after that, distilled water was used to rinse it. At 60°C, the colorless NiO compound was dried overnight to achieve a constant weight. After renewal AY99 NiO is now ready for the second-stage of absorption. The efficacy of renewal was discovered to be 97.6, 94.5, and 92.6% during each

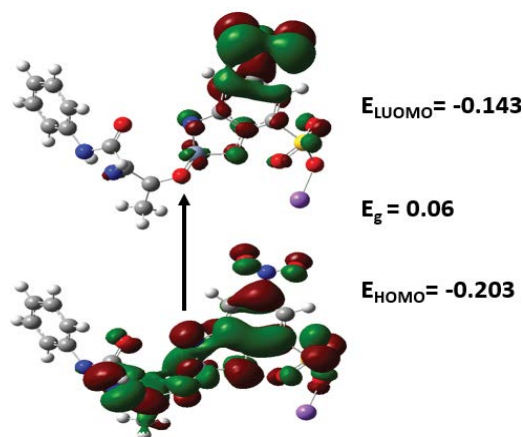


Fig. 15. The molecular orbital density distribution at the boundary of structures was optimized using AY99.

Table 8

The ability of various adsorbents to absorb the AY99 dye

Adsorbent	q_m (mg/g)	Reference
C-MM	121.8	[65]
MLP	708.15	[66]
MGMA-DETA	123.36	[67]
Cotton cellulose based cationic adsorbent	473.248	[68]
Coir pith	7.716	[69]
<i>Stipa Tenacissima</i> L cationized fibers	675.9	[70]
Cationized nylon	100.31	[71]
Cationized saw dust	279.32	[72]
Polyacrylonitrile/activated carbo composite	154.32	[73]
NiO	766.35	This work

cycle of adsorption/desorption this could be because NiO absorptions are restricted. We characterized the NiO material following three cycles of tests using XRD and discovered that the crystallinity and structure of the

substance were retained Fig. 16. Finding demonstrates that NiO nanoparticles have a high reusability rate. Eq. (7) was utilized to assess the effectiveness of the regeneration process:

$$\text{Regeneration efficiency (\%)} = \frac{\text{Total adsorption capacity in the second run}}{\text{Total adsorption capacity in the first run}} \times 100 \quad (7)$$

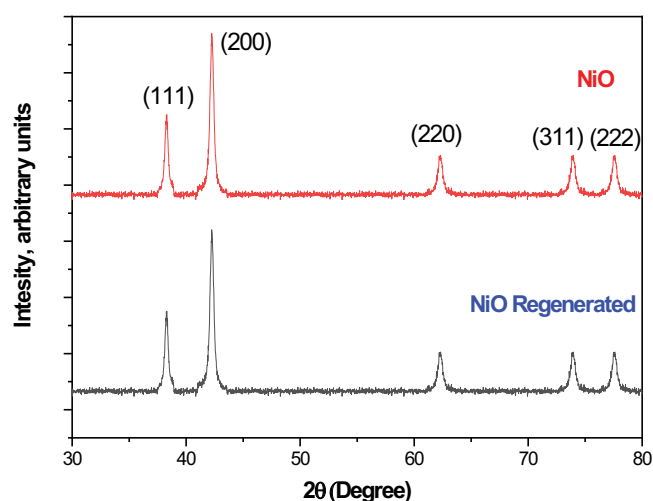


Fig. 16. XRD spectra of NiO at 450°C and NiO regenerated.

4. Conclusions

The ecology has been severely impacted by the indirect discharge of significant quantities of toxic dyes into water. Consequently, in this work, a technique to remove colours from industrial water was examined using to remove the dye AY99, NiO was created by calcining an organometallic chelate, which has a greater ability for adsorption in wastewater samples. NiO has extremely accessible surface areas, with typical pore sizes of 3.485 nm and 156.036 m²/g. The high-efficiency mesopores NiO catch AY99 dye from wastewater. The NiO adsorbent was significantly affected by the adsorption conditions, including the solution pH, which resulted in mesoporous surfaces with a potent ability to interact with and absorb AY99 dye. Adsorption tests demonstrated that NiO had a high capacity for the removal of AY99 (766 mg/g) and that this capacity was maintained even after numerous reuse cycles. Once adsorption equilibrium is taken into account, the Langmuir isotherm for AY99 more closely approximates the empirical data. The chemisorption approach is suggested by the mean adsorption energy (E_a), which is 24.8 kJ/mol. A pseudo-second-order kinetic model was shown to obey the adsorption kinetics as a result of the correlation coefficient (R^2). According to the thermodynamic calculations made (ΔH° , ΔS° , and ΔG°), AY99 adsorbs spontaneously and endothermically on NiO in the testing conditions. The mesoporous adsorbent proved a straightforward and efficient method for managing industrial effluent and water filtration. We believe that this work is the first to describe the use of NiO adsorbents for the elimination of AY99 dye from wastewater samples.

Acknowledgements

Princess Nourah bint Abdulrahman University Researchers Supporting Project number (PNURSP2022R76), Princess Nourah bint Abdulrahman University, Riyadh, Saudi Arabia.

Symbols

q_e	—	Adsorbed amount of dye at equilibrium concentration, mmol/g
q_{mL}	—	Maximum sorption capacity (corresponding to the saturation of the monolayer, mmol/g)
K_L	—	Langmuir binding constant which is related to the energy of sorption, L/mmol
C_e	—	Equilibrium concentration of dyes in solution
K_F	—	Freundlich constants related to the sorption capacity, (mmol/g)(L/mmol) ^{1/n}
n	—	Intensity
K_{DR}	—	Constant related to the sorption energy, J ² /mol ²
q_{DR}	—	Theoretical saturation capacity, mmol/g
ε	—	Polanyi potential, J ² /mol ²
R	—	Gas constant, 8.314 J/mol·K
T	—	Temperature where the adsorption occurs
A_T	—	Temkin isotherm constant
b_T	—	Temkin constant in relation to heat of adsorption, J/mol
q_i	—	Amount of dye adsorbed, mmol/g
K_1	—	Rate constant for pseudo-first-order constant for the adsorption processes, min ⁻¹
q_2	—	Maximum adsorption capacity for pseudo-second-order
K_2	—	Rate constant for pseudo-first-order constant for the adsorption processes, g/mg min
α	—	Chemical adsorption rate, mg/g·min
β	—	Coefficient in relation with extension of covered surface
ΔG°	—	Free Gibb's energy
ΔH°	—	Enthalpy
ΔS°	—	Entropy
K_c	—	Distribution coefficient
C_{eq}	—	Concentration at equilibrium, mg/L

References

- [1] N.M. Mahmoodi, M.H. Saffar-Dastgerdi, Clean laccase immobilized nanobiocatalysts (graphene oxide - zeolite nanocomposites): from production to detailed biocatalytic degradation of organic pollutant, *Appl. Catal., B*, 268 (2020) 118443, doi: 10.1016/j.apcatb.2019.118443.
- [2] W. Zou, L. Gong, M. Pan, Z. Zhang, C. Sun, H. Zeng, Effect of salinity on adsorption and interaction forces of hydrophobically modified polyacrylamide on silica and

- alumina surfaces, *Miner. Eng.*, 150 (2020) 106280, doi: 10.1016/j.mineng.2020.106280.
- [3] G. Yang, N. Song, F. Deng, J. Liang, Q. Huang, J. Dou, Y. Wen, M. Liu, X. Zhang, Y. Wei, Direct surface functionalization of graphene oxide with ionic liquid through gamma ray irradiation induced radical polymerization with remarkable enhanced adsorption capacity, *J. Mol. Liq.*, 306 (2020) 112877, doi: 10.1016/j.molliq.2020.112877.
- [4] D. Balarak, F. Mostafapour, Adsorption of acid red 66 dye from aqueous solution by heat-treated rice husk, *Res. J. Chem. Environ.*, 22 (2018) 80–84.
- [5] N.M. Mahmoodi, B. Hayati, M. Arami, Textile dye removal from single and ternary systems using date stones: kinetic, isotherm, and thermodynamic studies, *J. Chem. Eng. Data*, 55 (2010) 4638–4649.
- [6] N.M. Mahmoodi, F. Najafi, A. Neshat, Poly (amidoamine-co-acrylic acid) copolymer: synthesis, characterization and dye removal ability, *Ind. Crops Prod.*, 42 (2013) 119–125.
- [7] M.G. El-Desouky, M.A. Khalil, A.A. El-Bindary, M.A. El-Bindary, Biological, biochemical and thermochemical techniques for biofuel production: an updated review, *Biointerface Res. Appl. Chem.*, 12 (2022) 3034–3054.
- [8] M.G. El-Desouky, M. Abd El-Wahab, A.A. El-Bindary, Interpretations and DFT calculations for polypropylene/copper oxide nanosphere, *Biointerface Res. Appl. Chem.*, 12 (2022) 1134–1147.
- [9] B. Hayati, N.M. Mahmoodi, Modification of activated carbon by the alkaline treatment to remove the dyes from wastewater: mechanism, isotherm and kinetic, *Desal. Water Treat.*, 47 (2012) 322–333.
- [10] N.M. Mahmoodi, F. Moghimi, M. Arami, F. Mazaheri, Silk degumming using microwave irradiation as an environmentally friendly surface modification method, *Fibers Polym.*, 11 (2010) 234–240.
- [11] B. Zhang, Y. Wu, L. Cha, Removal of methyl orange dye using activated biochar derived from pomelo peel wastes: performance, isotherm, and kinetic studies, *J. Dispersion Sci. Technol.*, 41 (2020) 125–136.
- [12] M.S. Frost, M.J. Dempsey, D.E. Whitehead, The response of citrate functionalised gold and silver nanoparticles to the addition of heavy metal ions, *Colloids Surf., A*, 518 (2017) 15–24.
- [13] N.M. Mahmoodi, U. Sadeghi, A. Maleki, B. Hayati, F. Najafi, Synthesis of cationic polymeric adsorbent and dye removal isotherm, kinetic and thermodynamic, *J. Ind. Eng. Chem.*, 20 (2014) 2745–2753.
- [14] K. Mohajershojaei, N.M. Mahmoodi, A.J.B. Khosravi, Immobilization of laccase enzyme onto titania nanoparticle and decolorization of dyes from single and binary systems, *Biotechnol. Bioprocess Eng.*, 20 (2015) 109–116.
- [15] N.M. Mahmoodi, Photocatalytic degradation of dyes using carbon nanotube and titania nanoparticle, *Water Air Soil Pollut.*, 224 (2013) 1–8.
- [16] M. El-Bindary, M. El-Desouky, A.A. El-Bindary, Adsorption of industrial dye from aqueous solutions onto thermally treated green adsorbent: a complete batch system evaluation, *J. Mol. Liq.*, 346 (2021) 117082, doi: 10.1016/j.molliq.2021.117082.
- [17] N. Begletsova, E. Selifonova, A. Chumakov, A. Al-Alwani, A. Zakharevich, R. Chernova, E. Glukhovskoy, Chemical synthesis of copper nanoparticles in aqueous solutions in the presence of anionic surfactant sodium dodecyl sulfate, *Colloids Surf., A*, 552 (2018) 75–80.
- [18] S.H. Mosavi, R. Zare-Dorabei, M. Bereyhi, Rapid and effective ultrasonic-assisted adsorptive removal of Congo red onto MOF-5 modified by CuCl₂ in ambient conditions: adsorption isotherms and kinetics studies, *ChemistrySelect*, 6 (2021) 4432–4439.
- [19] M. Feng, L. Yan, X. Zhang, P. Sun, S. Yang, L. Wang, Z. Wang, Fast removal of the antibiotic flumequine from aqueous solution by ozonation: influencing factors, reaction pathways, and toxicity evaluation, *Sci. Total Environ.*, 541 (2016) 167–175.
- [20] J. Gomes, R. Costa, R.M. Quinta-Ferreira, R.C. Martins, Application of ozonation for pharmaceuticals and personal care products removal from water, *Sci. Total Environ.*, 586 (2017) 265–283.
- [21] M. Klavarioti, D. Mantzavinos, D. Kassinos, Removal of residual pharmaceuticals from aqueous systems by advanced oxidation processes, *Environ. Int.*, 35 (2009) 402–417.
- [22] E. Hapeshi, A. Achilleos, M.I. Vasquez, C. Michael, N.P. Xekoukoulotakis, D. Mantzavinos, D. Kassinos, Drugs degrading photocatalytically: kinetics and mechanisms of ofloxacin and atenolol removal on titania suspensions, *Water Res.*, 44 (2010) 1737–1746.
- [23] R. Hao, X. Xiao, X. Zuo, J. Nan, W. Zhang, Efficient adsorption and visible-light photocatalytic degradation of tetracycline hydrochloride using mesoporous BiOI microspheres, *J. Hazard. Mater.*, 209 (2012) 137–145.
- [24] J. Niu, Y. Xie, H. Luo, Q. Wang, Y. Zhang, Y. Wang, Cobalt oxide loaded graphitic carbon nitride as adsorptive photocatalyst for tetracycline removal from aqueous solution, *Chemosphere*, 218 (2019) 169–178.
- [25] G.A.A. Al-Hazmi, M.A. El-Bindary, M.G. El-Desouky, A.A. El-Bindary, Efficient adsorptive removal of industrial dye from aqueous solution by synthesized zeolitic imidazolate framework-8 loaded date seed activated carbon and statistical physics modeling, *Desal. Water Treat.*, 258 (2022) 85–103.
- [26] N.M. Mahmoodi, Synthesis of magnetic carbon nanotube and photocatalytic dye degradation ability, *Environ. Monit. Assess.*, 186 (2014) 5595–5604.
- [27] S.M. Khalaf, S.M. Al-Mahmoud, Adsorption of tetracycline antibiotic from aqueous solutions using natural Iraqi bentonite, *Egypt. J. Chem.*, 64 (2021) 3–4.
- [28] G.Z. Kyzas, J. Fu, N.K. Lazaridis, D.N. Bikiaris, K.A. Matis, New approaches on the removal of pharmaceuticals from wastewaters with adsorbent materials, *J. Mol. Liq.*, 209 (2015) 87–93.
- [29] N. Nasrollahi, S. Aber, V. Vatanpour, N.M. Mahmoodi, The effect of amine functionalization of CuO and ZnO nanoparticles used as additives on the morphology and the permeation properties of polyethersulfone ultrafiltration nanocomposite membranes, *Composites, Part B*, 154 (2018) 388–409.
- [30] N. Dhiman, N. Sharma, Removal of pharmaceutical drugs from binary mixtures by use of ZnO nanoparticles: (competitive adsorption of drugs), *Environ. Technol. Innovation*, 15 (2019) 100392, doi: 10.1016/j.eti.2019.100392.
- [31] M.A. El-Bindary, M.G. El-Desouky, A.A. El-Bindary, Metal-organic frameworks encapsulated with an anticancer compound as drug delivery system: synthesis, characterization, antioxidant, anticancer, antibacterial and molecular docking investigation, *Appl. Organomet. Chem.*, 36 (2022) e6660, doi: 10.1002/aoc.6660.
- [32] N. Hassan, A. El-Sonbati, M. El-Desouky, Synthesis, characterization, molecular docking and DNA binding studies of Cu(II), Ni(II), Zn(II) and Mn(II) complexes, *J. Mol. Liq.*, 242 (2017) 293–307.
- [33] N. Hassan, A. Shahat, A. El-Didamony, M. El-Desouky, A.A. El-Bindary, Synthesis and characterization of ZnO nanoparticles via zeolitic imidazolate framework-8 and its application for removal of dyes, *J. Mol. Struct.*, 1210 (2020) 128029, doi: 10.1016/j.molstruc.2020.128029.
- [34] M. Oveisi, M.A. Asli, N.M. Mahmoodi, Carbon nanotube based metal-organic framework nanocomposites: synthesis and their photocatalytic activity for decolorization of colored wastewater, *Inorg. Chim. Acta*, 487 (2019) 169–176.
- [35] A. Fouda, S.S. Salem, A.R. Wassel, M.F. Hamza, T.I. Shaheen, Optimization of green biosynthesized visible light active CuO/ZnO nano-photocatalysts for the degradation of organic methylene blue dye, *Heliyon*, 6 (2020) e04896.
- [36] F. Ramezani, R. Zare-Dorabei, Simultaneous ultrasonic-assisted removal of malachite green and methylene blue from aqueous solution by Zr-SBA-15, *Polyhedron*, 166 (2019) 153–161.
- [37] A. El-Bindary, S. El-Marsafy, A. El-Maddah, Enhancement of the photocatalytic activity of ZnO nanoparticles by silver doping for the degradation of AY99 contaminants, *J. Mol. Struct.*, 1191 (2019) 76–84.

- [38] S. Nourozi, R. Zare-Dorabe, Highly efficient ultrasonic-assisted removal of methylene blue from aqueous media by magnetic mesoporous silica; experimental design methodology, kinetic and equilibrium studies, *Desal. Water Treat.*, 85 (2017) 184–196.
- [39] N.M. Mahmoodi, B. Hayati, H. Bahrami, M. Arami, Dye adsorption and desorption properties of *Mentha pulegium* in single and binary systems, *J. Appl. Polym. Sci.*, 122 (2011) 1489–1499.
- [40] M.G. El-Desouky, A.A. El-Bindary, Magnetic metal-organic framework (Fe₃O₄@ZIF-8) nanocomposites for adsorption of anionic dyes from wastewater, *Inorg. Nano-Metal Chem.*, (2021) 1–15, doi: 10.1080/24701556.2021.2007131.
- [41] M.S. Tehrania, R. Zare-Dorabei, Highly efficient simultaneous ultrasonic-assisted adsorption of methylene blue and rhodamine B onto metal organic framework MIL-68 (Al): central composite design optimization, *RSC Adv.*, 6 (2016) 27416–27425.
- [42] A.S. Al-Wasidi, I.I. Al-Zahrani, A.M. Naglah, M.G. El-Desouky, M.A. Khalil, A.A. El-Bindary, M.A. El-Bindary, Effective removal of methylene blue from aqueous solution using metal-organic framework; modelling analysis, statistical physics treatment and DFT calculations, *ChemistrySelect*, 6 (2021) 11431–11447.
- [43] M.S. Tehrani, R. Zare-Dorabei, Competitive removal of hazardous dyes from aqueous solution by MIL-68(Al): derivative spectrophotometric method and response surface methodology approach, *Spectrochim. Acta, Part A*, 60 (2016) 8–18.
- [44] A.A. Mohammadi, A. Zarei, H. Alidadi, M. Afsharnia, M. Shams, Two-dimensional zeolitic imidazolate framework-8 for efficient removal of phosphate from water, process modeling, optimization, kinetic, and isotherm studies, *Desal. Water Treat.*, 129 (2018) 244–254.
- [45] N.M. Mahmoodi, A. Taghizadeh, M. Taghizadeh, M.A.S. Baglou, Surface modified montmorillonite with cationic surfactants: preparation, characterization, and dye adsorption from aqueous solution, *J. Environ. Chem. Eng.*, 7 (2019) 103243, doi: 10.1016/j.jece.2019.103243.
- [46] M.H. Dehghani, R.R. Karri, Z.T. Yeganeh, A.H. Mahvi, H. Nourmoradi, M. Salari, A. Zarei, M. Sillanpää, Statistical modelling of endocrine disrupting compounds adsorption onto activated carbon prepared from wood using CCD-RSM and DE hybrid evolutionary optimization framework: comparison of linear vs non-linear isotherm and kinetic parameters, *J. Mol. Liq.*, 302 (2020) 112526, doi: 10.1016/j.molliq.2020.112526.
- [47] T.A. Altalhi, M.M. Ibrahim, G.A.M. Mersal, M.H.H. Mahmoud, T. Kumeria, M.G. El-Desouky, A.A. El-Bindary, M.A. El-Bindary, Adsorption of doxorubicin hydrochloride onto thermally treated green adsorbent: equilibrium, kinetic and thermodynamic studies, *J. Mol. Struct.*, 1263 (2022) 133160, doi: 10.1016/j.molstruc.2022.133160.
- [48] I. Langmuir, The adsorption of gases on plane surfaces of glass, mica and platinum, *J. Am. Chem. Soc.*, 40 (1918) 1361–1403.
- [49] H. Freundlich, W. Heller, The adsorption of cis- and trans-azobenzene, *J. Am. Chem. Soc.*, 61 (1939) 2228–2230.
- [50] M.J. Temkin, V. Pyzhev, Recent modifications to Langmuir isotherms, *Acta Physiochim. URSS*, 12 (1940) 217–225.
- [51] M.M. Dubinin, E. Zaverina, L. Radushkevich, Sorption and structure of active carbons. I. Adsorption of organic vapors, *Zh. Fiz. Khim.*, 21 (1947) 151–162.
- [52] M. El-Desouky, M. El-Bindary, A. El-Bindary, Effective adsorptive removal of anionic dyes from aqueous solution, *Vietnam J. Chem.*, 59 (2021) 341–361.
- [53] S.K. Lagergren, About the theory of so-called adsorption of soluble substances, *Sven. Vetenskapsakad. Handlingar*, 24 (1898) 1–39.
- [54] Y.-S. Ho, G. McKay, Sorption of dye from aqueous solution by peat, *Chem. Eng. J.*, 70 (1998) 115–124.
- [55] D. Karatas, D. Senol-Arslan, O. Ozdemir, Experimental and atomic modeling of the adsorption of acid azo dye 57 to sepiolite, *Clays Clay Miner.*, 66 (2018) 426–437.
- [56] M.G. El-Desouky, A.A. El-Bindary, Magnetic metal-organic framework (Fe₃O₄@ZIF-8) nanocomposites for adsorption of anionic dyes from wastewater, *Inorg. Nano-Metal Chem.*, (2021) 1–15, doi: 10.1080/24701556.2021.2007131.
- [57] H.A. Kiwaan, F.Sh. Mohamed, A.A. El-Bindary, N.A. El-Ghamaz, H.R. Abo-Yassin, M.A. El-Bindary, Synthesis, identification and application of metal organic framework for removal of industrial cationic dyes, *J. Mol. Liq.*, 342 (2021) 117435, doi: 10.1016/j.molliq.2021.117435.
- [58] N.C. Corda, M. Srinivas Kini, A review on adsorption of cationic dyes using activated carbon, *MATEC Web Conf.*, 144 (2018) 02022, doi: 10.1051/mateconf/201814402022.
- [59] M.A. El-Bindary, M.G. El-Desouky, A.A. El-Bindary, Metal-organic frameworks encapsulated with an anticancer compound as drug delivery system: synthesis, characterization, antioxidant, anticancer, antibacterial and molecular docking investigation, *Appl. Organomet. Chem.*, 36 (2022) e6660, doi: 10.1002/aoc.6660.
- [60] M. El-Desouky, A. El-Bindary, M. El-Afify, N. Hassan, Synthesis, characterization, theoretical calculation, DNA binding, molecular docking, anticovid-19 and anticancer chelation studies of some transition metal complexes, *Inorg. Nano-Metal Chem.*, 52 (2022) 1–16.
- [61] N. Hassan, A. Shahat, A. El-Didamony, M. El-Desouky, A. El-Bindary, Equilibrium, kinetic and thermodynamic studies of adsorption of cationic dyes from aqueous solution using ZIF-8, *Moroccan J. Chem.*, 8 (2020) 2627–2637.
- [62] A.S. Al-Wasidi, I.I.S. Al-Zahrani, H.I. Thawibarak, A.M. Naglah, M.G. El-Desouky, M.A. El-Bindary, Adsorption studies of carbon dioxide and anionic dye on green adsorbent, *J. Mol. Struct.*, 1250 (2021) 131736, doi: 10.1016/j.molstruc.2021.131736.
- [63] A. Ashraf, M.G. El-Desouky, M.A.M. El-Afify, Thermal and spectroscopic studies of some prepared metal complexes and investigation of their potential anticancer and antiviral drug activity against SARS-CoV-2 by molecular docking simulation, *Biointerface Res. Appl. Chem.*, 12 (2021) 1053–1075.
- [64] M.G. El-Desouky, A.A. El-Bindary, M.A. El-Bindary, Low-temperature adsorption study of carbon dioxide on porous magnetite nanospheres iron oxide, *Biointerface Res. Appl. Chem.*, 12 (2021) 6252–6268.
- [65] N. Jović-Jovičić, P. Banković, Z. Mojović, B. Nedić-Vasiljević, S. Marinović, T. Mudrinić, A. Milutinović Nikolić, Ecologically friendly chitosan-montmorillonite bio-nanocomposite as adsorbent for textile dyes from aqueous solutions, *Sci. Sintering*, 49 (2017) 419–429.
- [66] M. Khan, R. Motiar, B. Sahoo, A.K. Mukherjee, A. Naskar, Biosorption of acid yellow-99 using mango (*Mangifera indica*) leaf powder, an economic agricultural waste, *SN Appl. Sci.*, 1 (2019) 1–15.
- [67] K. Elwakeel, A. El-Bindary, A. El-Sonbati, A. Hawas, Adsorption of toxic acidic dye from aqueous solution onto diethylenetriamine functionalized magnetic glycidyl methacrylate-N,N'-methylenebisacrylamide, *RSC Adv.*, 6 (2016) 3350–3361.
- [68] A.S. Patra, S. Ghorai, S. Ghosh, B. Mandal, S. Pal, Selective removal of toxic anionic dyes using a novel nanocomposite derived from cationically modified guar gum and silica nanoparticles, *J. Hazard. Mater.*, 301 (2016) 127–136.
- [69] V. Kumar, N. Goel, Y. Bhardwaj, S. Sabharwal, L. Varshney, Development of functional adsorbent from textile cotton waste by radiation induced grafting process: equilibrium and kinetic studies of acid dye adsorption, *Sep. Sci. Technol.*, 47 (2012) 1937–1947.
- [70] M.M.R. Khan, M. Ray, A.K. Guha, Mechanistic studies on the binding of Acid Yellow 99 on coir pith, *Bioresour. Technol.*, 102 (2011) 2394–2399.
- [71] A.E. Ghali, M.H.V. Baouab, M.S. Roudesli, *Stipa tenacissima* L cationized fibers as adsorbent of anionic dyes, *J. Appl. Polym. Sci.*, 116 (2010) 3148–3161.
- [72] M.H.V. Baouab, H. Zghida, R. Gauthier, H. Gauthier, Cationized nylon as adsorbent for anionic residual dyes, *J. Appl. Polym. Sci.*, 91 (2004) 2513–2522.
- [73] M.H.V. Baouab, R. Gauthier, H. Gauthier, M. El Baker Rammah, Cationized sawdust as ion exchanger for anionic residual dyes, *J. Appl. Polym. Sci.*, 82 (2001) 31–37.

Supporting information

S1. Chemicals

Chemicals have been used exactly as they were gathered, without any more processing. They 2,4-dihydroxy benzaldehyde (99%, Chemical Reagent of Tianjin Kemiou, China), cyanoacetate and piperidine Sinopharm Reagent Chemical Co., Ltd., in China), Merck KGaA, 64271, Darmstadt, Germany, purchased ammonium hydroxide solution (NH_3 , 25%–28%, Nanjing Chemical Reagent Co., Ltd., China), anhydrous ethanol (99.7%, Sinopharm chemical reagent Co., Ltd., China) and Acid Yellow 99 (AY99).

S1.1. Synthesis of NiO

S1.1.1. Synthesis of Cyano-6-(p-tolyl)azo-7-hydroxy coumarin (HL)

Two stages were used to make the ligand (HL): *Step 1*: Condensation of 2,4-dihydroxy benzaldehyde using ethyl cyanoacetate in the influence of piperidine yielded 3-cyano-7-hydroxy coumarin (0.01 mol). The media temperature was kept at 5°C by employing a salt bath with ice throughout adding, after that, the mixture was held at room temperature overnight before being put into a mixture of broken ice with stirring. The solid 3-cyano-7-hydroxy coumarin before recrystallization in ethanol, it was properly rinsed with cold water several times. *Step 2*: solutions that have been well-mixed of p-toluidine (0.02 mol) in 10 mL ethanol and 5 mL 2 M HCl was chilled in a bath in ice before diazotization with water sodium nitrite solution (5 mL, 0.01 mol). For 45 min, drop by drop additions of the diazonium solution that has been cooled (0–5°C) to a very well vigorous stirring of (0.01 mol) 3-cyano-7-hydroxy coumarin in (100 mL) ethanol containing sodium hydroxide (0.01 mol) were made. For another 30 min, the mixture was stirred before being refrigerated for 2 h. The solid was recovered, rinsed with water, and ethanol purified by recrystallization. The produced coumarin azo dye was subjected to elemental analysis and different spectroscopic techniques [22].

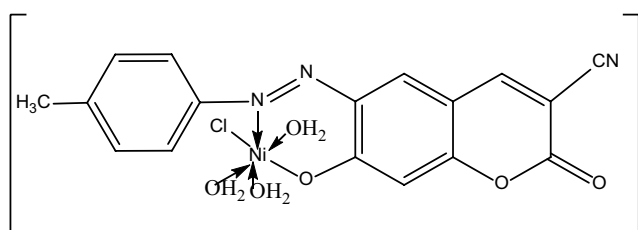


Fig. S1. Structure of Ni (II) complex.

S1.1.2. Synthesis of $[\text{Ni}(\text{L})\text{Cl}(\text{OH}_2)_3]$ complex

1 mmol of the ligand under investigation was reflux with 1 mmol of the metal salt ($\text{NiCl}_2 \cdot 6\text{H}_2\text{O}$) in an ethanolic solution on a water bath for 3 h yielded the Ni complex. With the adding of weak ammonia solution, the pH of the solution was kept at 5–6 (10 wt.%) Fig. S1. The resulting solid complexes were filtered off, rinsed several times in absolute ethanol, and then dried in desiccators over anhydrous calcium chloride [22].

S1.2. Characterization

FT-IR spectra (KBr discs, 4,000–400 cm^{-1}) by Jasco-4100 spectrophotometer. The structural differences of the as-prepared NiO were investigated using the X-ray diffraction (XRD) method. The powder XRD patterns were captured using a Siemens D-500 X-ray diffractometer equipped with a Cu K α source of radiation. UV-visible spectra from a Perkin-Elmer AA800 spectrophotometer Model AAS with a 1.0 cm model system. The pH meter utilized was a WTW 720 model digital pH meter. On ASAP 2020, the surface area was calculated to use the Brunauer–Emmett–Teller (BET) method, and the pore volume of the BET surfaces and the Barrett–Joyner–Halenda (BJH) surface were calculated (Micrometrics, USA). Scanning electron microscopy (JEOL, JSM7600F, Japan) was used to examine the microstructure of NiO. The specimen was then deposited onto a copper substrate after being sputter-coated with a homogenous gold layer. Energy-dispersive X-ray spectroscopy (EDX) was used to analyze the elemental distribution of NiO on a Leo1430VP microscope with a 5 kV operating voltage. XPS was measured using K-ALPHA (Thermo Fisher Scientific, USA).

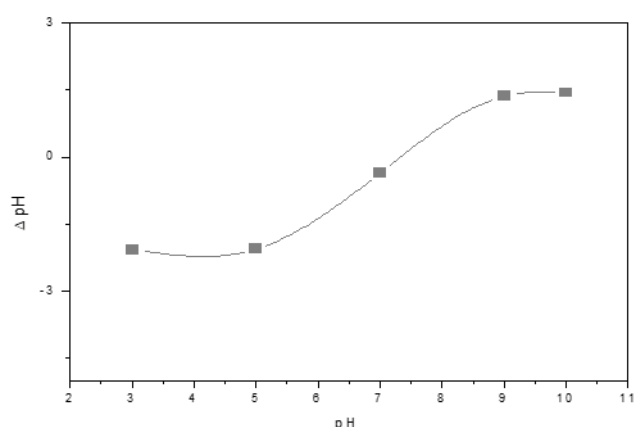


Fig. S2. Relation between initial pH and ΔpH of NiO.